ECS Transactions, 3 (15) 271-278 (2007)
10.1149/1.2721496, copyright The Electrochemical Society

Nucleation and Growth of Noble Metals on Oxide Surfaces Using Atomic Layer Deposition

J. W. Elam[a], A. V. Zinovev[a], M. J. Pellin[a], D. J. Comstock[b], and M. C. Hersam[b]

[a]Argonne National Laboratory, Argonne, Illinois 60439
[b]Department of Chemistry, Northwestern University, Evanston, Illinois 60208

Noble metals supported on metal oxide surfaces have broad applications in catalysis, microelectronics and sensing. In most applications it is critical to control the dispersion and morphology of the noble metals to achieve either a smooth, continuous film or isolated particles of controlled size. Here we examine the atomic layer deposition of Pd and Pt films onto a variety of metal oxide surfaces including Al_2O_3, ZrO_2, and TiO_2. *In situ* quartz crystal microbalance measurements and quadrupole mass spectrometry are used to explore the nucleation and growth of the Pd and Pt on the different metal oxide surfaces. Scanning electron microscopy and X-ray photoelectron spectroscopy are used to examine the morphology and surface state of the resulting Pt and Pd coatings. By varying the support material and the deposition conditions, we can control the morphology of the ALD noble metal coatings to yield agglomerated particles or continuous films.

Introduction

Noble metal layers supported on metal oxide surfaces have diverse applications ranging from catalysis to microelectronics. In many applications it is critical to control the morphology of the noble metal layer to obtain either a smooth, continuous film or an assembly of discrete particles. In catalytic and sensing applications, it is desirable to have noble metal nanoparticles with controlled size and dispersion. For instance, Pt nanoparticles supported on Yttria-stabilized zirconia are needed in solid oxide fuel cells[1], while Ag nanoparticles deposited on glass are used as optical sensors[2]. To be useful for microelectronics and conducting atomic force microscopy (C-AFM), the noble metal layer must be a smooth, continuous film. Examples include Ru films deposited onto (Pb-4%La)$(Zr_{0.3}Ti_{0.7})O_3$ for ferroelectric random access memories[3] and Pt films deposited on SiO_2 for C-AFM probes[4].

Atomic layer deposition (ALD) is a thin film growth technique that utilizes alternating, self-saturation chemical reactions between gaseous precursors and a surface to deposit materials in a layer-by-layer fashion[5]. ALD has been used previously to deposit a variety of noble metal films including Pt[6], Pd[7], Ru[8], Ir[9], and Rh[10]. In this manuscript, we describe the ALD of Pt and Pd films onto Al_2O_3, ZrO_2, and TiO_2 surfaces. Using *in situ* quartz crystal microbalance (QCM) and quadrupole mass spectrometry (QMS) measurements as well as *ex situ* analysis of films using scanning electron microscopy (SEM), x-ray photoelectron spectroscopy (XPS), and optical absorption, we show that the morphology of the noble metal films is influenced by the deposition conditions as well as the underlying substrate.

Experimental

The ALD films were deposited in a custom viscous flow reactor[11]. Ultrahigh purity nitrogen (99.999%) carrier gas was used at a mass flow rate of 360 sccm and a pressure of 1 Torr. Pd ALD[7] was performed using alternating exposures to palladium (II) hexafluoroacetylacetonate ($Pd(hfac)_2$, Aldrich) and formalin (HCOH, Aldrich) at a deposition temperature of 200°C. Pt ALD[6] was performed using alternating exposures to Trimethyl(methylcyclopentadienyl)platinum(IV) ($Pt(MeCp)Me_3$, Aldrich) and ultrahigh purity oxygen (99.999%) at a temperature of 300°C. The $Pd(hfac)_2$ and $Pt(MeCp)Me_3$ were held in stainless steel bubblers maintained at 50°C and 30°C, respectively. Ultrahigh purity nitrogen at a mass flow rate of 50-60 sccm was directed through the bubblers during the metal exposures, and was diverted to bypass the bubblers following the metal exposures. The ALD films were deposited onto 2 cmx2 cm Si(100) and glass substrates which were ultrasonically cleaned in acetone and then methanol prior to loading and subsequently cleaned *in situ* using a 60 s exposure to flowing ozone. For some of the samples, the substrates were first coated prior to the noble metal ALD with 10-100 nm of ALD Al_2O_3, ZrO_2 or TiO_2 using alternating exposures to TMA/H_2O, Bis(cyclopentadienyl)dimethyl Zirconium, $(ZrCp_2Me_2)/H_2O$ and $TiCl_4/H_2O$, respectively.

The ALD timing sequences can be expressed as t1-t2-t3-t4 where t1 is the exposure time for the first precursor, t2 is the purge time following the first exposure, t3 is the exposure time for the second precursor, t4 is the purge time following the exposure to the second precursor and all units are given in seconds (s). Typical timing sequences used for the ALD materials in these studies were 1-1-1-1 (Pd), 2-5-1-5 (Pt), 1-5-1-5 (Al_2O_3, TiO_2), and 2-5-1-5 (ZrO_2).

The Pd and Pd ALD were monitored *in situ* using quartz a crystal microbalance (QCM) and a quadrupole mass spectrometer (QMS). The QCM utilized a Maxtek BSH-150 bakeable sensor and AT-cut quartz sensor crystals with a polished front surface connected to a Maxtek TM400 film thickness monitor. The QMS (Stanford Research Systems RGA300) was located downstream of the QCM in a differentially-pumped chamber separated from the reactor tube by a 35 micron orifice and evacuated using a 50 l/s turbomolecular pump. The ALD metal oxide films that were applied to the Si(100) and glass substrates prior to the noble metal ALD also coated the QCM surface as well as all of the inner surfaces of the reactor. Consequently, the QCM and QMS measurements accurately probed the nucleation and growth of the noble metals on the metal oxide surfaces.

SEM images were acquired using an Hitachi S4700 SEM with a field emission gun electron beam source. Optical absorption measurements were performed on noble metal films deposited on glass slides using a J. A. Woolam Co. M2000 spectroscopic ellipsometer operated in transmission mode, and the absorption spectra were fit using optical constants supplied with the instrument to obtain the Pd and Pt film thicknesses. The thickness measurements obtained by optical absorption agreed well with thickness measurements obtained from cross sectional SEM. XPS measurements were made using MgKα (1253.6 eV) radiation and a hemispherical electron energy analyzer. ALD Pd was also deposited onto high surface area silica gel powder (Silicycle S10040T) with a specific surface area of 50 m^2/g and a pore size of 1000 Å. The Pd loadings on these samples were determined from X-ray fluorescence (XRF) measurements using an Oxford Instruments ED2000.

Results and Discussion

Palladium ALD

Figure 1a shows QCM measurements performed during Pd ALD on an Al_2O_3 surface using the timing sequence 1-1-1-1. The Pd deposition can be divided into two stages: nucleation (below ~100 cycles) during which the Pd film thickness changes very

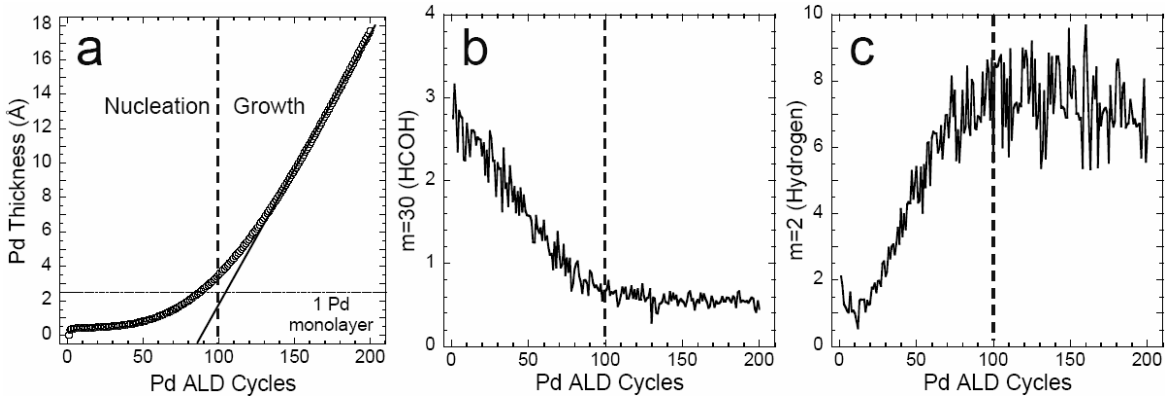

Figure 1: Pd nucleation and growth on Al_2O_3 at 200°C examined by QCM (a) and QMS (b,c).

slowly, and growth (above ~100 cycles) during which the Pd film thickness increases linearly with the number of cycles. This transition occurs at a Pd film thickness of ~1 Pd monolayer as indicated in Fig. 1a. In addition to using HCOH as the reducing agent for Pd ALD, we also tried hydrogen gas (H_2) which has been used previously for Pd ALD on noble metal surfaces[12]. We were unable to nucleate the Pd ALD on Al_2O_3 surfaces using H_2, however once a film had been nucleated using HCOH, we could continue the Pd deposition using H_2. We also used QMS to monitor the HCOH (m=30) and H_2 (m=2) signals during the HCOH exposures for Pd deposition on Al_2O_3. As shown in Figs. 1b and 1c, the HCOH signal decreases while the H_2 signal increases during the Pd nucleation, and both of these signals remain constant during the Pd growth. The behavior observed using the QMS can be explained by the decomposition of HCOH to form H_2 that occurs on Pd[13]:

$$HCOH \rightarrow H_2 + CO \quad \text{(Pd-catalyzed)} \qquad [1]$$

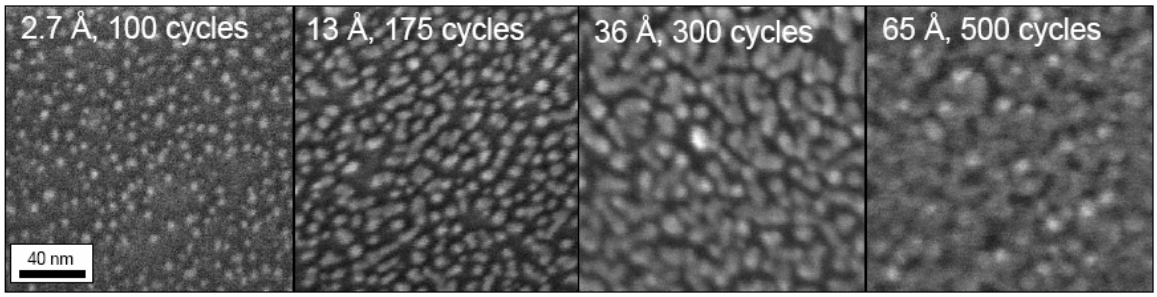

Figure 2: SEM images of ALD Pd films deposited on Al_2O_3 coated Si(100) substrates at 200°C versus number of Pd ALD cycles. The indicated Pd film thicknesses were determined using optical absorption measurements on glass substrates.

The rates of H_2 production and HCOH consumption are low initially because the Pd coverage is low. Both of these rates increase and then level off as the Pd nucleates and grows to cover the entire Al_2O_3 surface.

One explanation for the long Pd nucleation period (Fig. 1) can be found in the SEM images presented in Fig. 2. Clearly, the Pd ALD proceeds via the coalescence of islands on the Al_2O_3 surface. With increasing numbers of Pd ALD cycles, the Pd islands grow laterally until they coalesce and form a continuous film. The very low initial growth rate reflects the low density of Pd islands on the Al_2O_3, and may result from a low density of reactive sites for $Pd(hfac)_2$ adsorption on the Al_2O_3 surface. XPS analysis of these samples reveals residual fluorine from the $Pd(hfac)_2$ precursor covering ~10% of the surface. This fluorine contamination may also account for the long nucleation period because the fluorine may poison potential adsorption sites for the $Pd(hfac)_2$ precursor thereby limiting the density of initial island nucleation sites.

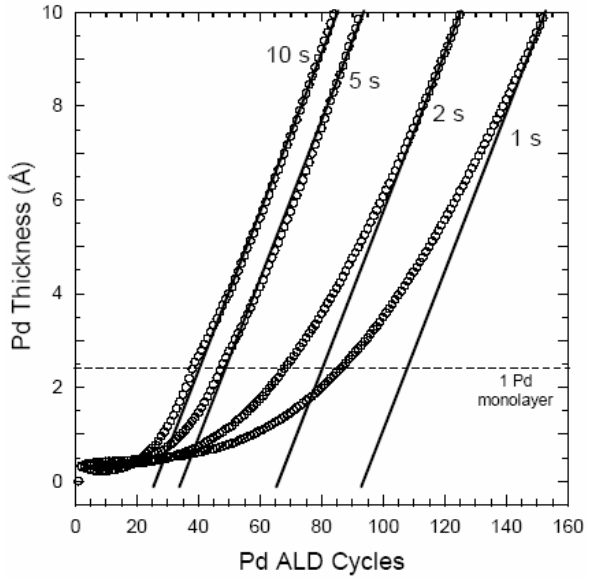

Figure 3: Effect of ALD Pd exposure times on the nucleation of ALD Pd on Al_2O_3 surface at 200°C measured by QCM. The different data sets were measured using ALD Pd exposure times of 1, 2, 5, and 10 s

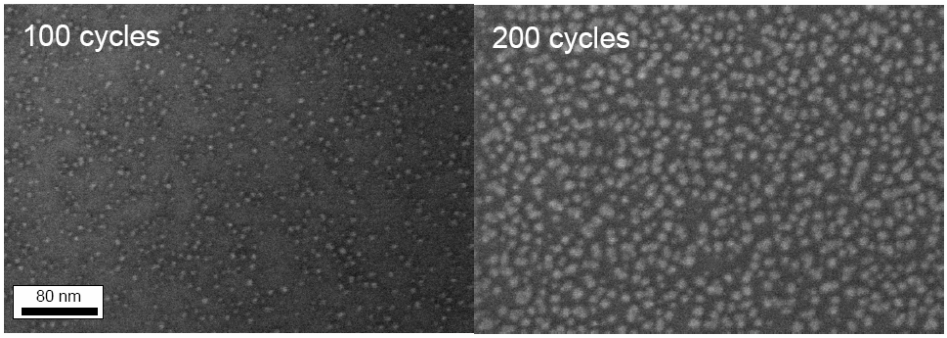

Figure 4: SEM images of ALD Pd films deposited on Al_2O_3 coated Si(100) substrates at 200°C using 1 ALD cycle with HCOH as the reducing agent, followed by 100 and 200 additional Pd ALD cycles using H_2 as the reducing agent.

We can affect the nucleation of the ALD Pd by controlling either the reactant exposure times or the reducing agent. For instance, Fig. 3 presents QCM measurements performed during Pd ALD on a previously-deposited ALD Al_2O_3 surface, and demonstrates that using progressively longer ALD exposure times of 1, 2, 5, and 10 s, the transition from nucleation to growth occurs at progressively lower numbers of ALD cycles. The accelerated nucleation observed using longer exposures should produce smoother, more continuous Pd films. Alternatively, we can enhance the tendency of the Pd to agglomerate by first nucleating the Pd ALD using formaldehyde for the initial ALD cycle, and then switching to hydrogen for the remaining ALD cycles. This process is illustrated by the SEM images in Figure 4. The Pd particles appear monodispersed after 100 cycles, but additional smaller Pd particles appear in the 200 cycle image indicating that some renucleation of new particles occurs using the H_2. This may result from residual HCOH in the valves and tubing used to supply both the H_2 and the HCOH.

The ALD Pd procedure used to coat the planar Si(100) and QCM sensor surfaces can also be employed to coat high surface area substrates relevant to catalysis. To demonstrate this capability, 0.5 g of silica gel powder was coated using 5 Al_2O_3 ALD cycles using the timing sequence 60-60-60-60 followed by 40 Pd ALD cycles using the timing sequence 100-25-100-25. The resulting powder was black in appearance and XRF analysis yielded a Pd loading of 9 wt%. SEM images of the Pd-coated silica gel reveal Pd nanoparticles (Fig. 5).

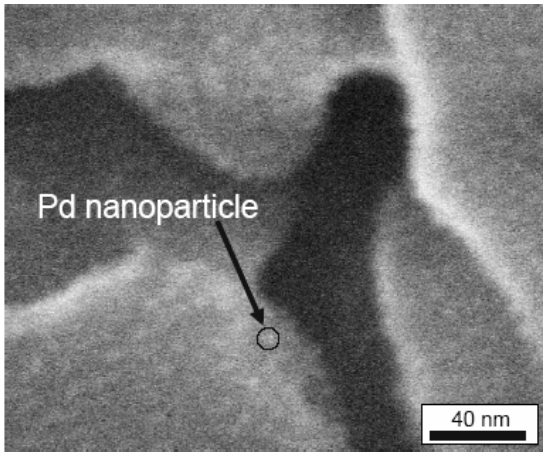

Figure 5: SEM image of silica gel powder coated with Pd nanoparticles by ALD.

Platinum ALD

Our initial Pt ALD experiments on Al_2O_3 surfaces revealed nucleation and growth behavior very similar to the Pd ALD described above. Using QCM and QMS measurements during the ALD of Pt on Al_2O_3, we observed a long incubation period followed by linear Pt growth similar to that depicted in Fig. 1. This behavior was confirmed by depositing Pt films onto glass and Si(100) substrates that had first been coated with 10 nm of ALD Al_2O_3. Optical absorption thickness measurements of the Pt films on glass revealed a nucleation period of ~75 cycles followed by linear growth. SEM images of the Pt films deposited concurrently on Si(100) substrates showed Pt particles that increase in size with the number of Pt ALD cycles performed such that the Pt film is nearly continuous after 75-100 cycles.

Following these initial studies on Al_2O_3 surfaces, we explored the nucleation of Pt on different metal oxide surfaces using QCM measurements and these results are shown in Fig. 6. It was found that the nucleation of ALD Pt on ZrO_2 was quite rapid, requiring only ~5 cycles to achieve linear growth as compared to ~30 cycles for Al_2O_3. In contrast, the nucleation of ALD Pt on TiO_2 was very slow, achieving a Pt thickness of only ~2 Å after 80 Pt ALD cycles.

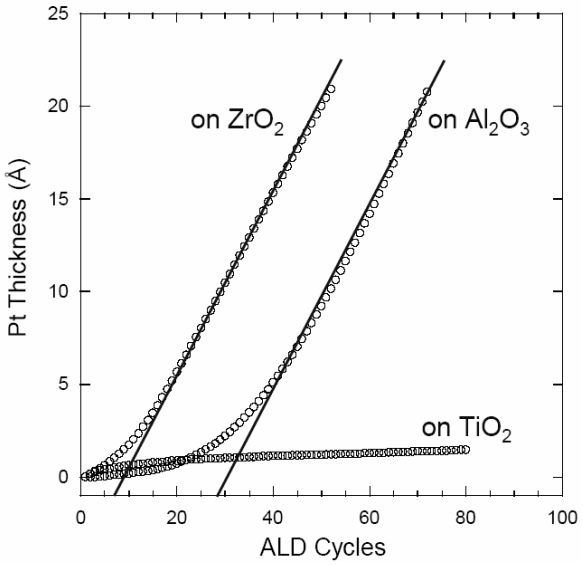

Figure 6: QCM measurements of Pt nucleation and growth on ZrO_2, Al_2O_3 and TiO_2 surfaces at 300°C.

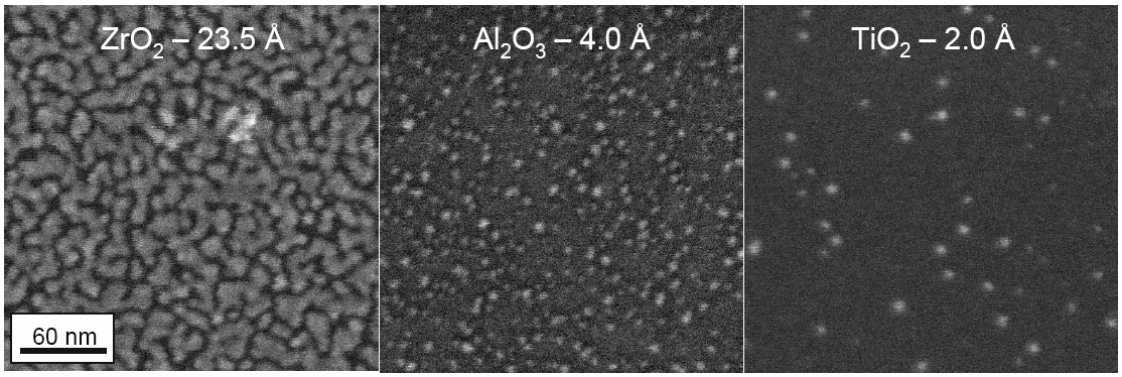

Figure 7. SEM images of ALD Pt deposited onto ZrO_2, Al_2O_3 and TiO_2 films on Si(100) substrates at 300°C. The indicated Pt film thicknesses were determined using optical absorption measurements on glass substrates.

To understand this behavior, we deposited ALD Pt films on Si(100) and glass substrates that had been previously coated with 5-10 nm Al_2O_3, ZrO_2, and TiO_2 by ALD. The Pt ALD was performed simultaneously on all of the metal oxide-coated samples for 40 Pt ALD cycles and SEM images of the Si(100) substrates are shown in Fig. 7. In agreement with the QCM measurements, we observed a nearly continuous Pt film on the ZrO_2 surface, almost no Pt on the TiO_2 surface, and high density of Pt particles on the Al_2O_3 surface. The Pt thicknesses indicated on the SEM images in Fig. 6 were obtained from optical absorption measurement of the Pt-coated glass substrates. This remarkable behavior suggests a much different reactivity of the $Pt(MeCp)Me_3$ precursor on the ZrO_2,

Al_2O_3, and TiO_2 surfaces. The failure of the Pt to grow on TiO_2 may result from surface poisoning by residual ligands from the $Pt(MeCp)Me_3$ precursor. XPS measurement performed on these samples could evaluate this hypothesis by measuring the relative amounts of surface carbon following Pt ALD on the different oxide surfaces.

Given that the Pt nucleates readily on ZrO_2, we can use ZrO_2 as a seed layer to achieve thin, continuous ALD Pt films as demonstrated in Fig. 8. Starting from a commercial Si AFM tip (Fig. 8b), we first apply 5 nm ALD ZrO_2 followed by 30 nm ALD Pt and the resulting Pt coating is smooth and conformal (Fig. 8c) in comparison to the rough, agglomerated Au coating for a commercial C-AFM tip (Fig. 8a). The smooth ALD Pt coating is expected to perform better than the agglomerated Au coating for conducting AFM applications.

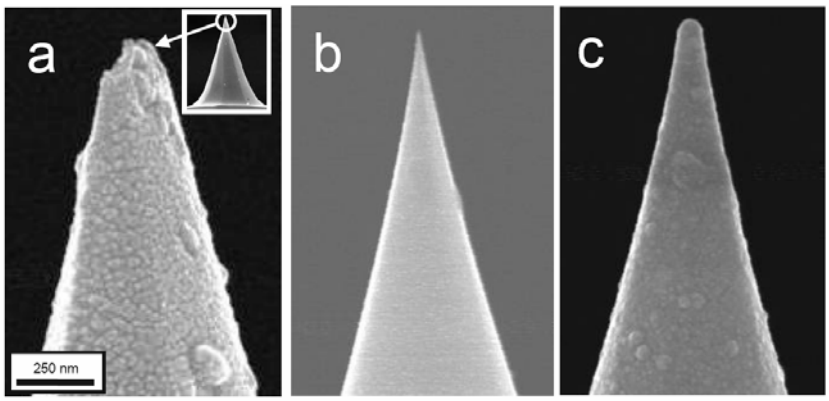

Figure 8. SEM images of (a) commercial Au-coated AFM tip, (b) uncoated Si AFM tip, and (c) the same Si AFM tip following 5 nm ALD ZrO_2 and 30 nm ALD Pt.

Conclusions

In this study, Pd and Pt noble metal layers were deposited by ALD onto a variety of metal oxide surfaces, and the morphology of the coatings could be controlled by altering the deposition conditions and the underlying substrate. Using *in situ* QCM and QMS measurements, we observed that the noble metal layers nucleate slowly on Al_2O_3 surfaces such that the ALD is divided into distinct nucleation and growth regimes. SEM images reveal that the Pd and Pt growth occurs by the coalescence of islands on the Al_2O_3 surfaces, and this behavior partially explains the incubation period observed in the QCM and QMS studies. The Pd nucleation can be accelerated by increasing the ALD exposure times, and agglomeration can be enhanced by switching the reducing agent from HCOH to H_2 after the first Pd ALD cycle. Nucleation during Pt ALD was found to depend strongly on the underlying metal oxide surface. Using identical Pt ALD conditions, nearly continuous Pt films were achieved on ZrO_2, a low density of isolated Pt nanoparticles formed on TiO_2, and Al_2O_3 showed an intermediate behavior with a high density of Pt nanoparticles. These findings have implications for a broad range of technologies ranging from catalysis to microelectronics.

Acknowledgements

The work at Argonne is supported by the U.S. Department of Energy, BES-Materials Sciences under Contract W-31-109-ENG-38. Electron microscopy was performed at the Electron Microscopy Center for Materials Research at Argonne National Laboratory, a U.S. Department of Energy Office of Science Laboratory operated under Contract No. DE-AC02-06CH11357 by UChicago Argonne, LLC.

References:

1. Y. I. Park, P. C. Su, S. W. Cha, Y. Saito and F. B. Prinz, *J. Electrochem. Soc.*, **153**, 2, A431, (2006).
2. A. J. Haes, S. L. Zou, G. C. Schatz and R. P. Van Duyne, *J. Phys. Chem. B*, **108**, 1, 109, (2004).
3. J. Bandaru, T. Sands and L. Tsakalakos, *J. Appl. Phys.*, **84**, 2, 1121, (1998).
4. M. Kitazawa and A. Toda, *Japanese Journal Of Applied Physics Part 1-Regular Papers Short Notes & Review Papers*, **41**, 7B, 4928, (2002).
5. M. Ritala and M. Leskela, in *Handbook of Thin Film Materials*, H. S. Nalwa, Editor, p. 103, Academic Press, San Diego, (2001).
6. T. Aaltonen, M. Ritala, T. Sajavaara, J. Keinonen and M. Leskela, *Chem. Mater.*, **15**, 9, 1924, (2003).
7. J. W. Elam, A. Zinovev, C. Y. Han, H. H. Wang, U. Welp, H. J. N and P. M. J, *Thin Solid Films*, **515**, 1664, (2006).
8. T. Aaltonen, P. Alen, M. Ritala and M. Leskela, *Chem. Vapor Depos.*, **9**, 1, 45, (2003).
9. T. Aaltonen, M. Ritala, S. V and M. Leskela, *J. Electrochem. Soc.*, **151**, 8, G489, (2004).
10. T. Aaltonen, M. Ritala and M. Leskela, *Electrochem. Solid-State Lett.*, **8**, 8, C99, (2005).
11. J. Elam, M. Groner and S. George, *Rev. Sci. Instrum.*, **73**, 8, 2981, (2002).
12. J. J. Senkevich, F. Tang, D. Rogers, J. Drotar, C. Jezewski, W. Lanford, G. Wang and T. Lu, *Chem. Vapor Depos.*, **9**, 5, 258, (2003).
13. K. H. Lim, Z. X. Chen, K. M. Neyman and N. Rosch, *J. Phys. Chem. B*, **110**, 30, 14890, (2006).